# *In-vivo* multicellular control of gene expression in microbial consortia

Davide Salzano[a,b], Barbara Shannon[b], Claire Grierson[c,d], Lucia Marucci[d,e,f*], Nigel J Savery[b,d*], Mario di Bernardo [a,g,*]

[a]*Scuola Superiore Meridionale, Naples, Italy*

[b] *School of Biochemistry, University of Bristol, United Kingdom*

[c] *School of Biological Sciences, University of Bristol, United Kingdom*

[d] *Bristol BioDesign Institute, University of Bristol, United Kingdom*

[e] *School of Engineering Mathematics and Technology, University of Bristol, United Kingdom*

[f] *School of Cellular and Molecular Medicine, University of Bristol, United Kingdom*

[g] *Department of Electrical Engineering and Information Technology, University of Naples Federico II, Italy*

* *These authors contributed equally*

[#] Correspondence should be addressed to: mario.di.bernardo@unina.it

**Keywords**: Cybergenetics, synthetic biology, control engineering, multicellular control, microbial consortia, gene regulation, Escherichia coli, modularity, biomedicine, industrial bioproduction.

**Abstract**

Cybergenetics, an emerging discipline straddling synthetic biology and control engineering, seeks to harness feedback control mechanisms for engineering reliable synthetic biological circuits that dynamically regulate target gene expression within host organisms. Current approaches, including embedded control strategies in both Escherichia coli and mammalian cells, suffer from limited modularity, requiring extensive re-engineering for controller design modifications. Furthermore, the challenge of engineering dependable microbial consortia remains a significant hurdle in synthetic biology and biotechnology. To address these limitations, we propose the concept of multicellular control, where distinct populations within a consortium perform specific tasks. In this paradigm, a controller population senses and computes real-time control actions to regulate processes within a second population, denoted as targets. Despite being theoretically proposed, in-vivo feasibility of multicellular control had remained unverified until now.

In this study, we propose for the first time a biological implementation and the experimental validation of multicellular control in a consortium of two Escherichia coli populations. Through comprehensive characterization, we demonstrate effective inter-population communication and behavioural influence, allowing the targets to achieve predetermined outcomes set by the controllers. Importantly, our approach enables tunable regulation of desired genes within the targets, showcasing robustness against perturbations, notably imbalances in population sizes.

Our innovative architecture not only establishes efficient cross-population communication but also offers adaptable gene regulation, even in the face of population imbalances. This advancement opens avenues for robust module development, with potential applications in

biomedicine and industrial bioproduction, marking a significant stride toward overcoming the challenges faced in the realm of synthetic biology and biotechnology.

## Introduction

Synthetic biology aims to engineer biomolecular systems to achieve new functions [1]; potential applications range from designing bacteria that can produce biofuels or sense and degrade pollutants in the environment (such as hydrocarbons and plastics), to immune cells that can track and kill cancer cells, or that can release drugs at specific points in desired conditions to avoid side effects (see [1] for an extensive review). Biomolecular feedback controllers have been highlighted as a crucial ingredient for reliable and robust synthetic biology devices [2]. Specifically, by applying concepts from control theory to guarantee desired static and dynamic performance of such devices, it is possible to drastically decrease the development time of new synthetic systems and to increase their flexibility and modularity [3, 4, 5].

Different designs have been proposed to implement biomolecular feedback control strategies both *in-silico* and *in-vivo*, ranging from simple feedback and feedforward loops to PID (Proportional Integral Derivative) controllers (see [3] and references therein). In particular, the introduction of an integral control action via an antithetic feedback motif has been highlighted as a fundamental ingredient for a synthetic circuit able to achieve and maintain a desired output even in the presence of disturbances [6], a property that has been termed *robust perfect adaptation* [5]. Integral biomolecular controllers have been thoroughly studied both theoretically [7] and experimentally, and different implementations have been proposed in bacteria [5] and mammalian cells [8]. For a review of the recent advancements in the implementations of biomolecular controllers guaranteeing robust perfect adaptation see [2].

However, existing robust controllers predominantly function at the single-cell level, posing inherent limitations on circuit complexity due to metabolic burdens and hindering their application as flexible plug-and-play modules across diverse synthetic and endogenous systems [6]. To overcome these constraints, a multicellular control strategy was conceived and computationally investigated [9]. In this approach, functionalities are distributed across distinct cell populations within a microbial consortium. Each cell strain encapsulates specific engineered gene networks, forming the foundation for a *distributed* feedback control loop [10] involving two populations: a controller population and a target cell population. The former

senses the targets' output, compares it with a reference signal encoding the desired expression level, and provides the latter with stimuli based on antithetic control logic [11, 12, 13, 14].

Following this work, in [15, 16] a biological implementation of a comparator, the logic core of the controller population, was designed and characterized both statically and dynamically but never tested *in vivo* with a target population. Further multicellular controllers were proposed (see [17] [18] and references within) but, to the best of our knowledge, the in-vivo implementation and validation of a distributed multicellular feedback control loop in a microbial consortium remains unexplored.

In this paper, we address this fundamental gap in the literature by developing and validating *in-vivo* a feedback control loop distributed across a bacterial consortium. We demonstrate its effectiveness in regulating a phenotype of interest in the target population even in the presence of variations in the consortium composition. This is achieved by designing two *Escherichia coli* strains embedding all the modules required to implement the three fundamental functions needed for control, namely computation, sensing and actuation [19]. We show that the designed cellular populations respond to their respective inputs and that the two populations can exchange information through two rationally designed communication channels, implemented using orthogonal quorum sensing signalling molecules. To demonstrate the validity of the proposed strategy, we carry out *in-vivo* experiments comparing the closed loop configuration, where the controller cells can sense the signalling molecules from the targets, with an open-loop implementation, where they cannot. Our results show that the proposed multicellular control approach can successfully be used to achieve reliable and robust regulation of the expression level of a gene of interest in the targets while guaranteeing robustness to composition imbalances in the consortium, a particularly important property for practical implementations.

## Results

### *A multicellular distributed control architecture*

The implementation of a multicellular control architecture requires the rational design of two populations, namely the *controllers* and the *targets* (see Figure 1a). The controllers receive

86 information about the targets' output ($y$) which is the expression level of some gene of interest
87 therein. This value is compared to that of some reference signal (*ref*) encoding the desired
88 expression level and a control input ($u$) is then generated via the designed control logic. This
89 signal is transmitted to the targets in order to regulate the level of their output to that encoded
90 by the reference. The communication between controllers and targets is implemented via
91 orthogonal Quorum Sensing molecules, where each cell population produces signalling
92 molecules that can diffuse through the growth environment and into the other population.

93 The control logic, embedded in the controllers, is an antithetic feedback control strategy [5],
94 based on the *in-silico* analysis presented in [9] and derived from the error computation module
95 (comparator) implemented *in-vivo* using molecular titration in [15] and characterized
96 dynamically in [16] . The controller network is a multi-input, single-output device that uses
97 two independent signals to regulate the expression level of its output protein (see Figure 1b).
98 It is constructed around a $\sigma$ factor [20], which is a protein that recruits RNA polymerase
99 (RNAP) to target promotors by binding to DNA sequences in the -10 and -35 regions of those
100 promoters , and their cognate anti-$\sigma$, which blocks the interaction between RNAP and the $\sigma$
101 factor by sequestering the $\sigma$ factor. The production of $\sigma$ is controlled by IPTG (the reference
102 signal), which induces expression from the promoter *plac-UV5*. The production of anti-$\sigma$ is
103 regulated by the *plux* promoter, which is activated by the complex formed by LuxR, produced
104 constitutively, and 3-O-C6-HSL, produced by the targets. The output signal of the controllers
105 (3-O-C12-HSL) is produced by the product of the *lasI* gene, which is regulated by the *p20 992*
106 promoter. This promoter, placed upstream of *lasI*, is induced by the presence of the orthogonal
107 $\sigma$ factor. The $\sigma$ and anti-$\sigma$ factors interact by binding and forming a complex that is unable to
108 recruit RNAP to *p20_992*. All proteins are fused to a degradation tag (ssrA tag) [21].

109 The targets can express a green fluorescent protein (GFP), whose expression level we aim to
110 regulate. The *gfp* gene is transcribed together with *luxI*, whose product is responsible for the
111 production of the molecule 3-O-C-6-HSL. This small molecule operates as a proxy of the *gfp*
112 expression levels by diffusing in the growth environment and activating the production of
113 anti-$\sigma$ in the controllers. The production of LuxI and GFP is regulated by *plas*. This promoter
114 is activated by the complex formed by LasR, which is constitutively expressed, and 3-O-C12-
115 HSL, which is produced by the controller population. In our implementation, LuxI was fused

116 to a degradation tag (ssrA tag) to ensure its fast degradation. All the details of the plasmids
117 and strains used in this work can be found in the *Strains and constructs* section of the Methods.

118 The goal of the design is to make the two engineered populations cooperate to steer and
119 maintain *gfp* expression in the targets at a desired setpoint level, which can be changed by
120 modifying the concentration of IPTG. Specifically, when *gfp* is overexpressed, the excessive
121 production of 3-O-C6-HSL upregulates the production of anti-$\sigma$. In turn, a reduction of the
122 free available $\sigma$, downregulates the production of LasI and, in turn, of the signalling molecule
123 3-O-C12-HSL. As a consequence, the activity of *pLas* in the targets should be reduced,
124 decreasing GFP expression levels. Similar mechanisms lead to an increase in GFP when GFP
125 falls below the desired level.

126 *Gene expression can be regulated via a multicellular architecture*

127 Prior to mixing the two populations in the consortium, we tested the functional modules
128 embedded in each population using flow cytometry [22]. Details on the machines and the
129 settings used can be found in section *Samples preparation and analysis using flow cytometry* of the
130 Methods.

131 We started by characterizing the response of the controller population to IPTG and 3-O-C6-
132 HSL, which are used in the architecture as a reference signal and a proxy for the targets state,
133 respectively. Note that, to measure the output level of the controllers, we substituted *lasI* with
134 a *gfp* fused with an ssrA tag (see Figure S1). We grew the controllers at 37 $^{o}$C for 3h adding
135 different concentrations of IPTG and 3-O-C6-HSL to the growth media to test their response
136 to their inputs. The fluorescence levels of the population was then analysed by Flow
137 Cytometry (for more details see section *Induction protocol* of the Methods). The addition of
138 IPTG promoted *plac-UV5* activity by inhibiting the repression exerted by LacI, thus inducing
139 up to 300 fold increase in the steady state fluorescence when 100 $\mu M$ IPTG was added to the
140 media (Figure 2a). Conversely, the addition of 3-O-C6-HSL increased the anti-$\sigma$ level of
141 transcription by activating *plux;* as a consequence, the fluorescence levels consistently
142 decreased, resulting in the inhibition of *gfp* expression levels up to 100 folds when 100 nM 3-
143 O-C6-HSL was added to the growth media (Figure 2a). We used the same procedure to assess
144 the response of the targets to 3-O-C12-HSL; as expected, addition of 10 $\mu M$ 3-O-C12 in the
145 growth media promoted *plas* activity and a 14 fold increase was detected in average GFP

146 fluorescence (Figure 2b). These assays confirmed that the controllers were correctly
147 responding to changes either in the reference signal or in the output of the targets, and,
148 confirmed that the targets were able to adjust GFP production according to the concentration
149 of 3-O-C12-HSL. For further details on the standard deviation of the response of targets and
150 controllers see Figure S2.

151 We then assayed the ability of the two populations to communicate with each other. To test
152 the ability of the controllers to stimulate the targets in the absence of any feedback from the
153 latter, we implemented an open loop configuration of the consortium where the output
154 sensing module was removed from the controller cells (see Figure 2c, right panel). This made
155 them unable to receive feedback sensing molecules from the targets. We will refer to this
156 population as *open loop controllers*.

157 We mixed the open loop controllers with the targets every hour, grew the consortium at 37 $^{o}$C
158 for 6h and analysed the targets fluorescence via flow cytometry (for further details on the
159 experimental protocol see section *Time-course assays* of the methods). This time course,
160 reported in Figure 2d (light blue trajectory), shows that the open loop controllers are able to
161 communicate with the targets, i.e. that the 3-O-C12-HSL is successfully produced by the open
162 loop controllers and sensed by the targets. Indeed, the controllers were able to induce a 15
163 fold increase in the average fluorescence of the targets after 6h. However, over this time period
164 the open loop controllers were not able to stabilize the *gfp* expression levels in the targets
165 confirming that, as expected, they were unable to receive any feedback signal sent from them.
166 We performed a similar experiments mixing the controllers with the targets. In closed loop,
167 where controllers possess the module to sense the expression level of the controlled gene in
168 the targets, stabilization of the targets fluorescence was observed after 3h (Figure 2d, yellow
169 trajectory). This confirms that the targets were able to successfully produce 3-O-C6-HSL
170 molecules which were correctly received by the controller population.

171 We then tested the ability of the controllers in the closed loop configuration to regulate *gfp*
172 expression levels in the targets to different values by modulating the concentration of IPTG in
173 the culture medium. Specifically, we grew controllers and targets in coculture at 37 $^{o}$C for 6h,
174 both with and without IPTG in the growth medium and then analysed the fluorescence level
175 of the targets using flow cytometry. When the consortium was induced with 50 $\mu$M IPTG, the

176 relative increase in fluorescence was approximately 50% (Figure 2e). This increase was
177 surprisingly small compared to the expected increase in the output observed during the
178 preliminary characterisation of the populations. Comparing the 6h timepoint of the closed
179 loop time course without IPTG shown in Figure 2d with the uninduced targets response
180 shown in Figure 2b, we observed that the targets were expressing high levels of fluorescence
181 when mixed with the controllers, even when no IPTG was present in the culture media (Figure
182 S3 shows a comparison of the distribution of fluorescence of the targets in the two scenarios).
183 This suggests that there was an unexpected high basal production of 3-O-C12-HSL, which was
184 not revealed during the initial characterisation of the populations shown in Figure 2a. The
185 inability to reveal the base expression level in the initial characterisation highlights the
186 difference between the expression level needed to detect any GFP signal and the levels of
187 enzyme needed to produce enough signalling molecules to induce the targets.

188 We addressed this problem by reducing the synthesis rate of $\sigma$ in the absence of IPTG, aiming
189 to increase the range of GFP fluorescence levels we could regulate the targets to. Specifically,
190 we increased the repression efficiency of *plac-UV5* by LacI by adding an extra lac operator
191 upstream of the promoter. This, as shown in [23], reduces the basal expression of the gene
192 controlled by LacI enabling the LacI tetramer to bind two operators simultaneously, thus
193 increasing the apparent affinity of the interaction (see *strains and constructs* section of the
194 methods for more details on the construction of the plasmid). We will henceforth denote the
195 modified controllers/open loop controllers "controllers/open loop controllers 2.0". After
196 adding the extra operator, the steady state fluorescence of the targets in closed loop and open
197 loop was reduced to levels that were lower than the ones reached by uninduced target
198 monocultures after 6h of growth (see Figure 3a,b). This indicated that the addition of the extra
199 operator reduced dramatically the leakiness of the *plac-UV5* promoter. We then repeated the
200 dynamic characterisation of the open and closed loop configurations of the consortium using
201 the new version of both controller populations. In open loop, the open loop controllers 2.0
202 were able to stabilize *gfp* expression levels in the targets after 6h. In addition, by increasing
203 the IPTG concentration in the culture media, we could achieve up to a 10-fold increase in GFP
204 expression levels. However, the regulation was highly variable across the different biological
205 replicates, especially at 0 $\mu M$ and 3 $\mu$M IPTG (see Figure 3a). By closing the feedback loop with
206 the addition of the output sensing module in the controllers, we were able to increase the

207 reliability of the regulation, reducing the standard deviation at the 6h timepoint 5-fold and
208 29-fold, when we used 0 $\mu$M and 3 $\mu$M IPTG, respectively. In addition, the settling time was
209 comparable to the open loop configuration (approximately 3h), and we were able to induce
210 up to a 5-fold increase when 7 $\mu$M IPTG was added to the culture medium (see Figure 3b).

211 We further investigated the tunability of the regulation in both configurations by analysing
212 the steady state response with increasing levels of IPTG (details of the protocol used can be
213 found in the *Titration assays* section of the Methods). Specifically, we mixed the
214 controllers/open loop controllers 2.0 with the targets and grew the consortium for 6h at 37 $^{o}$C.
215 Figure 3c shows that both consortia were able to regulate the *gfp* gene to different expression
216 levels. Both architectures showed saturation when IPTG $\in [0\ \mu M; 2\ \mu M]$. Above that
217 concentration, increases in IPTG concentrations drove an increase in the targets' fluorescence
218 levels. In addition, both consortia underwent an abrupt increase in the targets' average
219 fluorescence and in its variance when we used IPTG at concentrations above $8\mu M$. Using the
220 remaining data (IPTG $\in [2\ \mu M,\ 8\ \mu M]$), where the response of both systems was mostly linear,
221 we observed some differences in the regulation patterns between the two configurations. The
222 closed loop system showed an almost linear increase in GFP fluorescence, while in open loop
223 we noticed a sharp increase in fluorescence levels between 2μM and 3μM IPTG, followed by
224 much flatter increase in fluorescence when IPTG was present at concentrations above 5 $\mu M$.
225 We quantified the linearity of the input-output response of both configurations to IPTG by
226 fitting the data with linear least square estimators and comparing the $R^2$ values. Using the
227 data where IPTG $\in [2\ \mu M, 8\ \mu M]$, the estimator fitting the closed loop data (yellow dashed line
228 in Figure 3c) predicts almost perfectly the variance coming from the data ($R^2$ = 0.927). In
229 contrast, the estimator that fits the data obtained using the open loop configuration of the
230 consortium explained just above half of such variance ($R^2$ = 0.624).

231 In our experiments, we established the effectiveness of a multicellular control architecture in
232 regulating the expression of a desired gene within the target population. Our findings
233 underscore the significant impact of feedback incorporation, leading to a substantial reduction
234 in response variability and enhanced linearity in the input-output relationship of the
235 architecture.

236 *Closed loop control enhances robustness to changes in the consortium composition*

237 A crucial problem when multicellular strategies are deployed in a consortium across multiple
238 cellular populations [24] is that different populations may grow at different rates because of
239 differences in their metabolic loads. This may hinder the ability of the controllers to steer the
240 dynamics of the targets as it might cause fluctuations in the production rate of the sensing (3-
241 O-C6-HSL) and actuation (3-O-C12-HSL) molecules. We therefore analysed the robustness of
242 both the closed loop and the open loop configurations to changes in the consortium
243 composition (see Figure 4).

244 We produced consortia of different compositions by inoculating targets and controllers/open
245 loop controllers 2.0. in different ratios, then measuring the average fluorescence of the targets
246 after 6h (for more detail see section *Consortium composition assay* of the Methods). Figure 4 a-d
247 shows that varying the proportion of controllers2.0 and targets had no detectable effect on the
248 reliability of the regulation of the closed loop configuration where feedback between the two
249 populations is present. Conversely, in the absence of feedback (in the open-loop
250 configuration), we noted a declining trend in the fluorescence levels of the targets as the
251 percentage of targets increased, especially when 0 μM and 3 μM IPTG concentrations were
252 employed. This trend was not seen when 5 $\mu M$ and 7 $\mu$M IPTG were present in the culture
253 medium. We quantified the difference between the fluorescence of the targets depending on
254 their percentage in the consortium by fitting linear least square estimators to the data (dashed
255 lines in Figure 4 a-d). We then compared the slopes of the lines fitting the open and closed
256 loop datapoints at different IPTG concentrations (see Figure 4 e). Using analysis of covariance
257 and a multiple comparison test, we found that when 0μM and 3μM IPTG were used, the
258 slopes of the linear models fitting the closed and open loop datapoints were statistically
259 different with $p$-values equal to 0.01527 and 1.13 $10^{-6}$, respectively. In contrast, when 5μM
260 and 7μM IPTG were present in the culture media, the changes were not significant. This could
261 be attributed to the saturation of the *plas* promoter activity at higher IPTG concentrations,
262 which reduced the sensitivity of the targets to variations in the 3-O-C12-HSL concentration
263 (see Supplementary Figure S4 for more details and section S1 of the Supplementary
264 Information for the details on the protocol used).

265 The analysis was finalized by conducting a statistical comparison of the slopes of the curves
266 fitted to the closed-loop data points across all IPTG concentrations. Employing the same

methodology, we established that there were no significant differences in slopes within the closed-loop system (detailed p-values provided in Table S3). This confirmed the consistent robustness of the multicellular feedback control strategy in maintaining stability, even in the presence of imbalances between the controllers' and targets' populations.

## Discussion

Our study presents for the first time the *in-vivo* biological implementation of synthetic feedback controllers within cellular populations, using a multicellular control architecture where, withing a consortium, a specific population of controller cells possesses the ability to sense and regulate targeted phenotypes within another population of cells. This strategic distribution of control functionalities across members of a microbial consortium alleviates the metabolic burden that would otherwise be imposed if all functions were concentrated within a single cell, as noted in prior research [5]. Moreover, this approach enhances the consortium's robustness, enabling it to adapt effectively to changes in its composition.

Following the validation of individual components within our microbial community, we meticulously assessed the architecture's performance and robustness using flow cytometry. Our results unequivocally demonstrate the distributed feedback controller's capability to effectively regulate gene expression within target cells, maintaining the desired levels even in the face of alterations in the consortium's composition. To substantiate the effectiveness of our control architecture, we conducted a comparative analysis between open and closed loop implementations. This examination clearly underscores the pivotal role of feedback mechanisms, revealing that their incorporation significantly enhances both the reliability and robustness of gene regulation within the system.

The development of distributed feedback controllers across microbial communities paves the way for the construction of complex interacting communities, where each population carries out a specific function [25]. Implementation of our distributed consortia within microfluidics/microscopy platforms would allow the realisation of more complex feedback control tasks in space and time [26] [27] [16].

296 Such microbes could be used in applications ranging from the integration of bacteria in the
297 human gut microbiome to treat a class of diseases [28] to engineering the soil microbiome to
298 increase plant growth and health [29], and bacteria-based production of fuels, which presents
299 a promising source for sustainable energy [30].

300 Current theoretical work is aimed at improving the performance and robustness of the
301 proposed design by expanding the consortium to include additional controller populations,
302 adding, for example, populations able to implement proportional or derivative control actions
303 in order to achieve a multicellular implementation of biomolecular PID controllers recently
304 proposed in [31], [32].

305 **Methods**

306 *Strains and constructs*

307 *Escherichia coli* strain TOP10 was used for all the cloning manipulations of this work.
308 *Escherichia coli* strain MG1655 $\lambda$-, rph-1 [33] was used for all the assays in this work and
309 transformed with the plasmids constituting either the controllers or the targets. For all the
310 sequences of the primers and the synthesised genes used in this study see Table S1, Table S2.
311 In addition, all the maps of the plasmids are reported In Figure S5.

312 The controllers contain three plasmids: pVRa20_992_BS2 (medium copy number),
313 pVRc20_992_BS1 (medium copy number) and pVRb_LasI (low copy number). The genes
314 constituting the essential core of the computation module ($\sigma$, anti-$\sigma$ and lasI) are ssrA tagged
315 (AANDENYALAA) to ensure fast dynamics of expression and degradation [21].

316 pVRb_lasI encodes the *lasI* gene, under the control of the *p_20992* promoter, and was built in
317 [15], together with pVRb_ssrA, where the lasI gene was swapped with a superfolder *gfp*.
318 pVRb_lasI was present in the controllers in each of the assays where they were mixed with
319 the targets, whereas pVRb_ssra was present in the controllers for their input output
320 characterisation.

321 Vector backbones for pVRa20_992_BS2 and pVRc20_992_BS1 were derived from plasmids
322 pVRa20_992 and pVRc20_992 [20]. pVRa20_992_BS2 produces a $\sigma$ factor under the control of
323 a promoter that responds to IPTG.. To construct this plasmid, first the pVRa20_992_BS1
324 plasmid was obtained by standard restriction digestion and ligation procedure, by amplifying

325 the $\sigma$ gene from the pLusB plasmid [15] with primers Sigma_plus_tag_F and
326 Sigma_plus_tag_R and cloning the PCR product in the pVRa_20_992 plasmid after
327 NcoI/BamHI digestion. Then, the *plac* promoter was substituted with *plac-UV5* to obtain the
328 pVRa20_992_BS2 plasmid. The construct was built by standard restriction digestion and
329 ligation procedure, by amplifying *plac-UV5* from the pVRa_placASb_Flag plasmid [15] with
330 primers PlacUV5_F and PlacUV5_R and cloning the PCR product in pVRa_20_992_BS1
331 plasmid after XbaI digestion. Finally, we modified pVRa_20_992_BS2 by introducing a second
332 lac operator upstream of *plac_UV5*. This construct, denoted as PVRa_20_992_DS, was
333 constructed by Gibson assembly after PCR amplification of pVRa20_992_BS2 using primers
334 Back_extralac_for and Back_extralac_rev, and of the pVRbLacO1O1Del from [34] using the
335 Ins_extralac_for and Ins_extralac_rev primers. pVRc20_992_BS1 produces the anti-$\sigma$ factor
336 under the induction of 3-O-C6-HSL. The plasmid was constructed by standard restriction
337 digestion and ligation procedure, by amplifying anti-$\sigma$ from pVRa_placASb_Flag [15] with
338 primers Anti_Sigma_plus_tag_F and Anti_Sigma_plus_tag_R and cloning the PCR product
339 in pVRc_20_992 plasmid after BamHI/PstI digestion. Finally, the controllers expressing a Red
340 Fluorescent Protein were implemented by substituting the pVRb_lasI plasmid with the
341 pVRb_lasI_RFP plasmid. pVRb_lasI_RFP was assembled using standard restriction digestion
342 and ligation procedure, by amplifying a synthetically generated RFP with primers
343 RFP_Afe_for and RFP_Nde_rev and cloning the PCR product in the pVRb_lasI plasmid after
344 AfeI/NdeI digestion.

345 The targets hosted p_Las_Lux_GFP_3.0, a plasmid that embeds the 3-O-C12-HSL inducible
346 promoter *plas,* driving the expression of a mut3 green fluorescent protein and of the luxI gene
347 (fused with and ssrA tag). This plasmid was assembled by Gibson assembly after PCR
348 amplification of the las_composite_device plasmid from [35] with
349 p_Las_Lux_GFP_3_0_fwd_20 and p_Las_Lux_GFP_3_0_rev_20 primers, and of the luxI from
350 pTeLu_GFP constructed in [15] with the luxI_fwd and luxI_rev primers.

351 *Chemicals*

352 For all experiments, kanamycin (50 $\mu$g/mL), ampicillin (100 $\mu$g/mL) and chloramphenicol (25
353 $\mu$g/mL) were added to the growth media, depending on the bacteria selective resistance. These
354 antibiotics were supplied by Sigma-Aldrich. pVRa_20992_BS2 and pVRa_20_992_DS have an

355 Ampicillin resistant gene, pVRb_lasI, pVRB_lasI_RFP and pVRb_ssrA have a gene conferring
356 Kanamycin resistantce, and pVRc_20_992_BS1 and p_Las_Lux_GFP_3.0 have a gene
357 guaranteeing Chroranmphenicol resistance. When multiple populations were mixed, the
358 antibiotics to which both populations were resistant were used. If no resistance was in
359 common, no antibiotic was used.

360 3-O-C6-HSL (N-(B-Ketocaproyl)-L-Homoserine Lactone from Sigma-Aldrich, cat # K3007)
361 and 3-O-C12-HSL (N-(3-Oxododecanoyl)-L-homoserine lactone from Sigma-Aldrich, cat #
362 O9139) were dissolved in DMSO, filter-sterilized and added to the LB growth medium at the
363 indicated concentrations. IPTG (Isopropyl $\beta$-D-1-thiogalactopyranoside, supplied by Sigma-
364 Aldrich, cat # I5502) was dissolved in water, filter-sterilized and added to LB medium at the
365 indicated concentrations.

366 *Samples preparation and analysis using flow cytometry*

367 Each sample (0.5 mL volume) was resuspended in 1xPBS and diluted to achieve a final $OD_{600}$
368 for the culture of 0.05. Data were acquired using either BD LSRFortessa X-20 or Acea Novocyte
369 flow cytometer. The results analysed using FlowJo.

370 The events recorded by a flow cytometer were first gated in the forward scatter (FSC-H, proxy
371 of cellular size), side scatter (SSC-H, proxy of cellular complexity) plane. Here, the events were
372 divided in three subpopulations: healthy cells where size and complexity were in
373 physiological ranges [36], stressed cells where the bacteria had increased size and complexity
374 due to filamentation, and cellular debris corresponding to events with high size with respect
375 to their complexity (Figure S6 a). Subsequently, healthy cells were gated in the SSC-H, SSC-A
376 plane to select for single cells. Cells with comparable signals in the two channels were selected
377 as single cells, whereas events with much larger SSC-A were classified as cellular
378 conglomerates and excluded from the analysis (Figure S6b). Finally, single cells were gated
379 using the FITC-H (Novocyte machine)/FITC-A (Fortessa machine) (490 nm excitation, 530/30
380 nm emission) channel to discriminate targets and controllers based on their fluorescence
381 levels. Specifically, cells with low FITC-H signal were classified as controllers and cells having
382 high FITC-H fluorescence were selected to be targets (Figure S6c). Alternatively, when
383 controllers constitutively expressed RFP, events with a high signal in the PE-CF594 (560 nm

384 excitation, 610/20 nm emission filter, Red) channel were distinguished as controllers while
385 cells with low signal were designated as targets.

386 *Induction protocol*

387 Cells were cultured in 10 mL LB broth in 50 mL Falcon tubes. 20$\mu L$ of overnight cultures were
388 added to the media, which was supplemented with the inducer(s) at the specified
389 concentration. The culture was then incubated at 37 $^{o}C$, shaking at 250rpm for 3h. Then, the
390 samples were prepared and analysed by flow cytometry. This protocol was used to obtain
391 Figures 2 a,b.

392 *Time-course assays*

393 35 $\mu L$ of overnight cultures of controllers and 140 $\mu L$ of overnight cultures of targets were
394 separately diluted each in 35 mL LB added to a 250mL sterile flask. Each culture was
395 supplemented with the specified concentration of IPTG. Both cultures were incubated at 37
396 $^{o}$C, shaking at 250rpm for 6h. Each hour, 5 mL of both cultures were mixed in sterile 50 mL
397 tubes, which were then incubated alongside the single strain cultures. After 6h, 0.5 mL of all
398 mixed cultures were sampled and analysed via flow cytometry. Note that the hours in Figure
399 2c and Figure 3a,b refer to the time targets and controllers have been mixed for. Figure 2c
400 Figure 3a,b were obtained using this protocol.

401 *Titration assay*

402 For each condition, 8$\mu L$ of overnight culture of targets and 2$\mu L$ of overnight culture of
403 controllers were mixed in 10 mL LB broth in 50 mL Falcon tubes. Each culture was
404 supplemented with IPTG at the specified concentration. The cultures were then incubated at
405 37 $^{o}C$, shaking at 250rpm for 6h. Then, the samples were prepared and analysed by flow
406 cytometry. This protocol was used to obtain Figure 3 c.

407 *Consortium composition assay*

408 Overnight cultures of targets and controllers were diluted in 10 mL LB using different
409 targets:controllers ratios. Specifically, 15:1, 8:1, 4:1, 2:1, 1:1 ratios were created by adding 10$\mu L$
410 of controllers and 150 $\mu L$, 80 $\mu L$, 40 $\mu L$, 20 $\mu L$, 10 $\mu L$ of targets, respectively. All cultures were

411 incubated at 37 °C shaking at 250rpm for 6h. Then, 0.5 mL of each culture was sampled and
412 analysed by flow cytometry. This protocol was used in Figure 2d, Figure 4a-d.

413

414 **Data availability**

415 The authors declare that the data supporting the findings of this study are available within
416 the paper and its Supplementary Information files or from the corresponding author on
417 reasonable request. The source data underlying all figures in the main text and supplementary
418 information are provided as a Source Data file.

419

420 **Acknowledgements**

421 The authors wish to acknowledge Gwen Brouwer and Abigail Smith for their support with
422 the cloning of the constructs needed for this work. Also, the authors also wish to
423 acknowledge the FACS facility hosted at the University of Bristol for their support with the
424 use of the Flow Cytometers. M.d.B., L.M. wish to acknowledge support from the European
425 Project FET-OPEN Cosy-Bio (Grant Agreement number 766840). M.d.B. also wishes to
426 acknowledge support from the PNRR and PNC projects of the Italian Government. L.M.
427 acknowledges funding from the Engineering and Physical Sciences Research Council
428 (EPSRC, Fellowship EP/S01876X/1) and the Biotechnology and Biological Sciences Research
429 Council (BrisEngBio grant, BB/W013959/1). Finally, L.M., N.J.S., C.G. and M.d.B. wish to
430 acknowledge support form BrisSynBio, a BBSRC/EPSRC Synthetic Biology Research Centre
431 (BB/L01386X/1).

432

433 **Author Contributions**

434

435 M.d.B, L.M., N.J.S. and C.G. designed the research; D.S. designed the experiments; D.S. and
436 B.Scarried out the experiments; D.S. with support from M.d.B., L.M., N.J.S. and C.G. analyzed
437 the data; D.S. and M.d.B. wrote the manuscript with inputs from L.M., N.J.S. and C.G.

## Competing Interests

The authors declare no competing interests.

References


[1] D. D. Vecchio, Y. Qian, R. M. Murray and E. D. Sontag, "Future systems and control research in synthetic biology," Annual Reviews in Control, vol. 45, p. 5–17, 2018.

[2] M. Filo, C.-H. Chang and M. Khammash, "Biomolecular feedback controllers: from theory to applications," Current Opinion in Biotechnology, vol. 79, p. 102882, February 2023.

[3] M. Khammash, M. D. Bernardo and D. D. Bernardo, "Cybergenetics: Theory and Methods for Genetic Control System," in 2019 IEEE 58th Conference on Decision and Control (CDC), 2019.

[4] M. Chevalier, M. Gómez-Schiavon, A. H. Ng and H. El-Samad, "Design and Analysis of a Proportional-Integral-Derivative Controller with Biological Molecules," Cell Systems, vol. 9, p. 338–353.e10, October 2019.

[5] S. K. Aoki, G. Lillacci, A. Gupta, A. Baumschlager, D. Schweingruber and M. Khammash, "A universal biomolecular integral feedback controller for robust perfect adaptation," Nature, vol. 570, p. 533–537, June 2019.

[6] I. Ruolo, S. Napolitano, D. Salzano, M. di Bernardo and D. di Bernardo, "Control engineering meets synthetic biology: Foundations and applications," Current Opinion in Systems Biology, vol. 28, p. 100397, December 2021.

[7] C. Briat, C. Zechner and M. Khammash, "Design of a Synthetic Integral Feedback Circuit: Dynamic Analysis and DNA Implementation," ACS Synthetic Biology, vol. 5, p. 1108–1116, July 2016.

[8] T. Frei, C.-H. Chang, M. Filo, A. Arampatzis and M. Khammash, "A genetic mammalian proportional–integral feedback control circuit for robust and precise gene regulation," Proceedings of the National Academy of Sciences, vol. 119, June 2022.

[9] G. Fiore, A. Matyjaszkiewicz, F. Annunziata, C. Grierson, N. J. Savery, L. Marucci and M. di Bernardo, "In-silico Analysis and Implementation of a Multicellular Feedback Control Strategy in a Synthetic Bacterial Consortium," ACS Synthetic Biology, vol. 6, p. 507–517, December 2016.

[10] F. Bullo, J. Cortés and S. Martinez , Distributed control of robotic networks: a mathematical approach to motion coordination algorithms., Princeton University Press, 2009.

[11] P. Bittihn, M. O. Din, L. S. Tsimring and J. Hasty, "Rational engineering of synthetic microbial systems: from single cells to consortia," Current Opinion in Microbiology, vol. 45, p. 92–99, October 2018.

[12] A. Guarino, D. Fiore, D. Salzano and M. di Bernardo, "Balancing Cell Populations Endowed with a Synthetic Toggle Switch via Adaptive Pulsatile Feedback Control," ACS Synthetic Biology, vol. 9, p. 793–803, March 2020.

[13] D. Fiore, D. Salzano, E. Cristobal-Coppulo, J. M. Olm and M. di Bernardo, "Multicellular Feedback Control of a Genetic Toggle-Switch in Microbial Consortia," IEEE Control Systems Letters, vol. 5, p. 151–156, January 2021.

[14] E. Weill, V. Andreani, C. Aditya, P. Martinon, J. Ruess, G. Batt and F. Bonnans, "Optimal control of an artificial microbial differentiation system for protein bioproduction," in 2019 18th European Control Conference (ECC), 2019.

[15] F. Annunziata, A. Matyjaszkiewicz, G. Fiore, C. S. Grierson, L. Marucci, M. di Bernardo and N. J. Savery, "An Orthogonal Multi-input Integration System to Control Gene Expression in Escherichia coli," ACS Synthetic Biology, vol. 6, p. 1816–1824, July 2017.

[16] B. Shannon, C. G. Zamora-Chimal, L. Postiglione, D. Salzano, C. S. Grierson, L. Marucci, N. J. Savery and M. di Bernardo, "In Vivo Feedback Control of an Antithetic Molecular-Titration Motif in Escherichia coli Using Microfluidics," ACS Synthetic Biology, vol. 9, p. 2617–2624, September 2020.

[17] G. Perrino, A. Hadjimitsis, R. Ledesma-Amaro and G.-B. Stan, "Control engineering and synthetic biology: working in synergy for the analysis and control of microbial systems," Current Opinion in Microbiology, vol. 62, p. 68–75, August 2021.

[18] N. S. McCarty and R. Ledesma-Amaro, "Synthetic Biology Tools to Engineer Microbial Communities for Biotechnology," Trends in Biotechnology, vol. 37, p. 181–197, February 2019.

[19] K. J. Åström and R. M. Murray, Feedback Systems An Introduction for Scientists and Engineers, Second Edition, Princeton University Press, 2021, p. 528.

[20] V. A. Rhodius, T. H. Segall-Shapiro, B. D. Sharon, A. Ghodasara, E. Orlova, H. Tabakh, D. H. Burkhardt, K. Clancy, T. C. Peterson, C. A. Gross and C. A. Voigt, "Design of orthogonal genetic switches based on a crosstalk map of σ anti- σ and promoters," Molecular Systems Biology, vol. 9, p. 702, January 2013.

[21] K. E. McGinness, T. A. Baker and R. T. Sauer, "Engineering Controllable Protein Degradation," Molecular Cell, vol. 22, p. 701–707, June 2006.

[22] K. M. McKinnon, "Flow Cytometry: An Overview," Current Protocols in Immunology, vol. 120, January 2018.

[23] S. Oehler, E. R. Eismann, H. Krämer and B. Müller-Hill, "The three operators of the lac operon cooperate in repression.," The EMBO Journal, vol. 9, p. 973–979, April 1990.

[24] D. Salzano, D. Fiore and M. di Bernardo, "Ratiometric control of cell phenotypes in monostrain microbial consortia," Journal of The Royal Society Interface, vol. 19, July 2022.

[25] N. E. Grandel, K. R. Gamas and M. R. Bennett, "Control of synthetic microbial consortia in time, space, and composition," Trends in Microbiology, vol. 29, p. 1095–1105, December 2021.

[26] I. de Cesare, D. Salzano, M. di Bernardo, L. Renson and L. Marucci, "Control-Based Continuation: A New Approach to Prototype Synthetic Gene Networks," ACS Synthetic Biology, vol. 11, p. 2300–2313, June 2022.

[27] E. Pedone, I. de Cesare, C. G. Zamora-Chimal, D. Haener, L. Postiglione, A. L. Regina, B. Shannon, N. J. Savery, C. S. Grierson, M. di Bernardo, T. E. Gorochowski and L. Marucci, "Cheetah: A Computational Toolkit for Cybergenetic Control," ACS Synthetic Biology, vol. 10, p. 979–989, April 2021.

[28] I. Y. Hwang and M. W. Chang, "Engineering commensal bacteria to rewire host–microbiome interactions," Current Opinion in Biotechnology, vol. 62, p. 116–122, April 2020.

[29] Y. Arif, P. Singh, H. Siddiqui, A. Bajguz and S. Hayat, "Salinity induced physiological and biochemical changes in plants: An omic approach towards salt stress tolerance," Plant Physiology and Biochemistry, vol. 156, p. 64–77, November 2020.

[30] T. S. Bayer, D. M. Widmaier, K. Temme, E. A. Mirsky, D. V. Santi and C. A. Voigt, "Synthesis of Methyl Halides from Biomass Using Engineered Microbes," Journal of the American Chemical Society, vol. 131, p. 6508–6515, April 2009.

[31] M. Filo, S. Kumar and M. Khammash, "A hierarchy of biomolecular proportional-integral-derivative feedback controllers for robust perfect adaptation and dynamic performance," Nature Communications, vol. 13, April 2022.

[32] V. Martinelli, D. Salzano, D. Fiore and M. di Bernardo, "Multicellular PI Control for Gene Regulation in Microbial Consortia," IEEE Control Systems Letters, vol. 6, p. 3373–3378, 2022.

[33] M. S. Guyer, R. R. Reed, J. A. Steitz and K. B. Low, "Identification of a Sex-factor-affinity Site in E. coli as," Cold Spring Harbor Symposia on Quantitative Biology, vol. 45, p. 135–140, January 1981.

[34] A. J. Smith, F. Thomas, D. Shoemark, D. N. Woolfson and N. J. Savery, "Guiding Biomolecular Interactions in Cells Using de Novo Protein-Protein Interfaces," ACS Synthetic Biology, vol. 8, p. 1284–1293, May 2019.

[35] N. Kylilis, Z. A. Tuza, G.-B. Stan and K. M. Polizzi, "Tools for engineering coordinated system behaviour in synthetic microbial consortia," Nature Communications, vol. 9, July 2018.

[36] D. F. Ackerley, Y. Barak, S. V. Lynch, J. Curtin and A. Matin, "Effect of Chromate Stress on Escherichia coli K-12," Journal of Bacteriology, vol. 188, p. 3371–3381, May 2006.

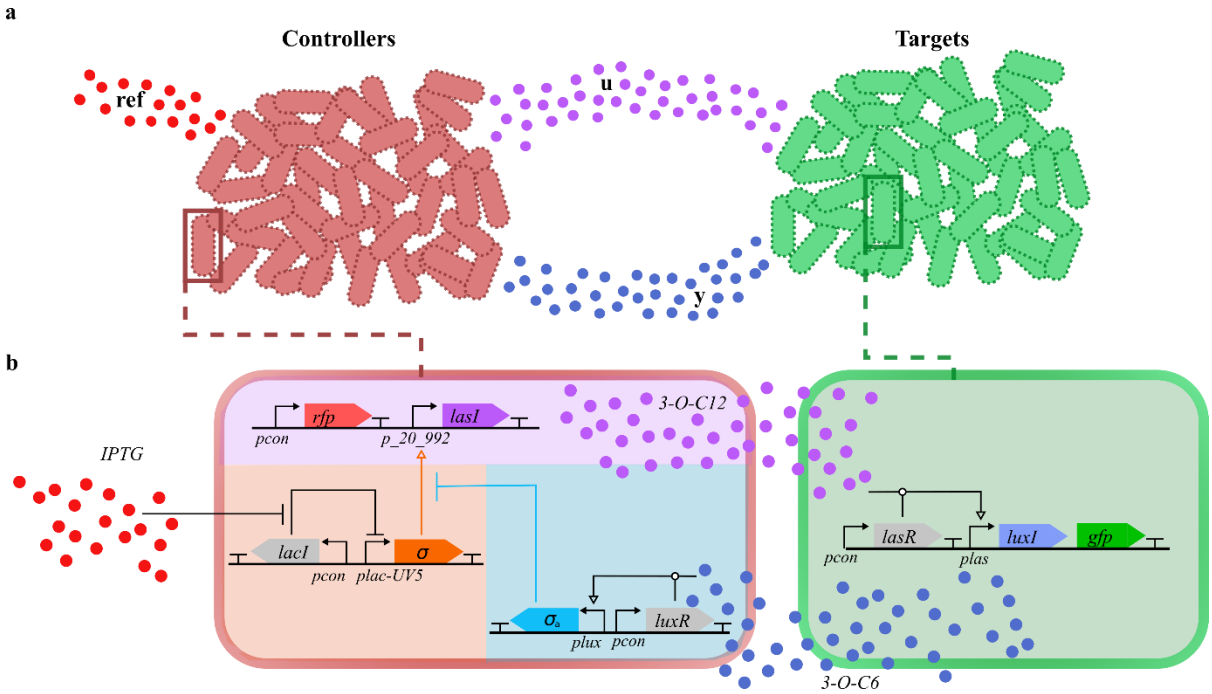


Figure 1 **Multicellular control schematic. A** Microbial consortium implementing a multicellular control architecture. The two populations, i.e. controllers and targets, share information using orthogonal quorum sensing channels (**u** and **y**), playing the role of the control input and the output of the process, respectively. In addition, the controllers sense the external stimulus labeled as **ref,** used to set up the reference of the feedback loop. **b.** Biological implementation of the multicellular control architecture. The Synthetic Biology Open Language (SBOL) notation is used to denote promoters, genes, promotion/inhibition relationships and quorum sensing molecules. The shaded areas identify different functional modules within each population.

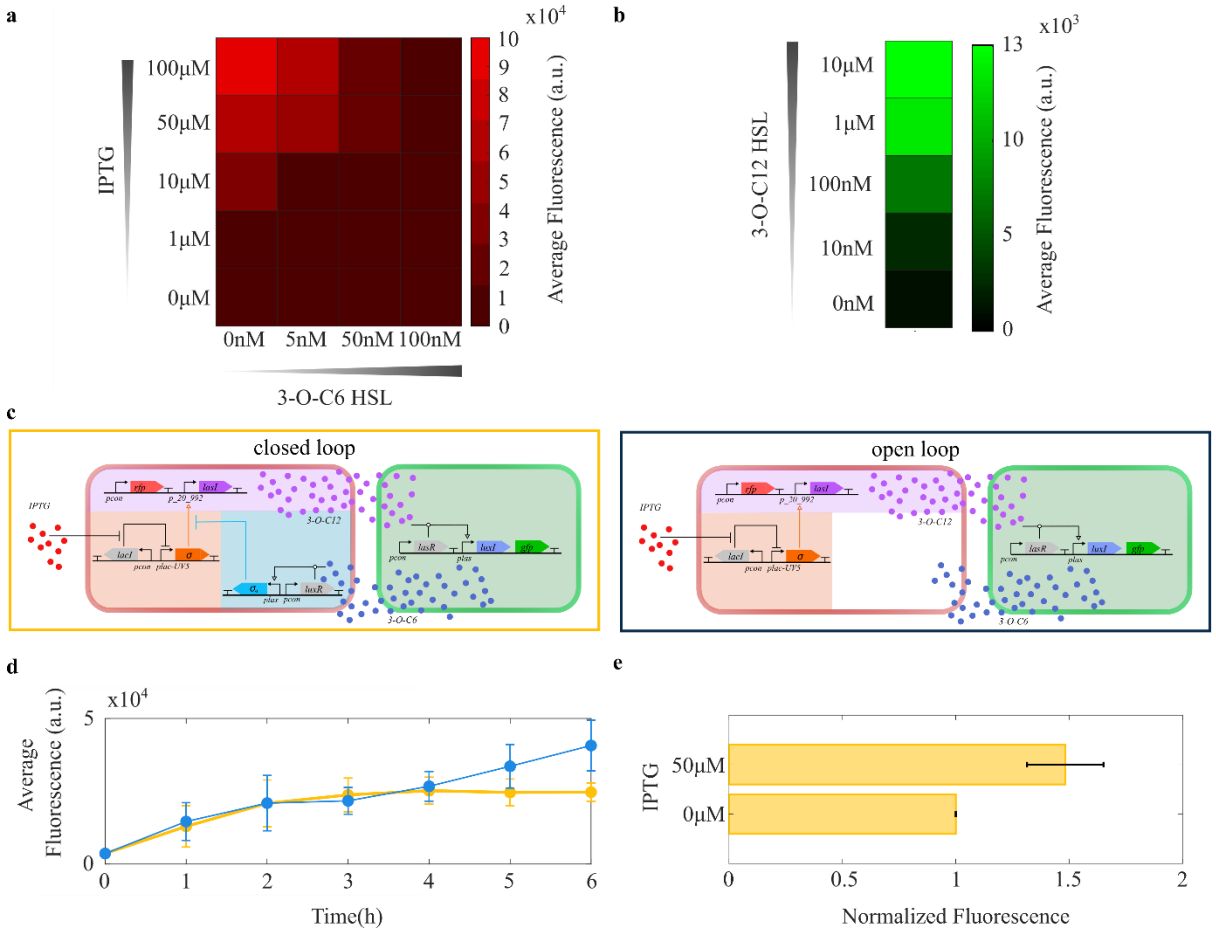


Figure 2 **Characterization of the controllers and targets cell populations. a:** Average fluorescence of the controller population induced using different concentrations of 3-O-C6-HSL and IPTG. The data were collected after 3h from the initial inoculation. **b:** Average fluorescence levels of the target population induced using 3-O-C12-HSL. The data were collected after 3h from the initial inoculation. **c:** Schematic representation of the closed loop (left) and the open loop (right) configurations. **d:** Average fluorescence of the targets over a 6h time course in open (blue) and closed (yellow) loop. The solid dots and vertical bars represent the average and standard deviation over n=3 biological replicates, respectively. **e:** Normalized average fluorescence of the targets mixed with the controllers in closed loop when 0 $\mu$M and 50 $\mu$M IPTG were present in the growth media. The data were collected 6h after the initial inoculation. The fluorescence was normalized to the average fluorescence reached when no IPTG was added in the media. All data are averaged over n=3 biological replicates.

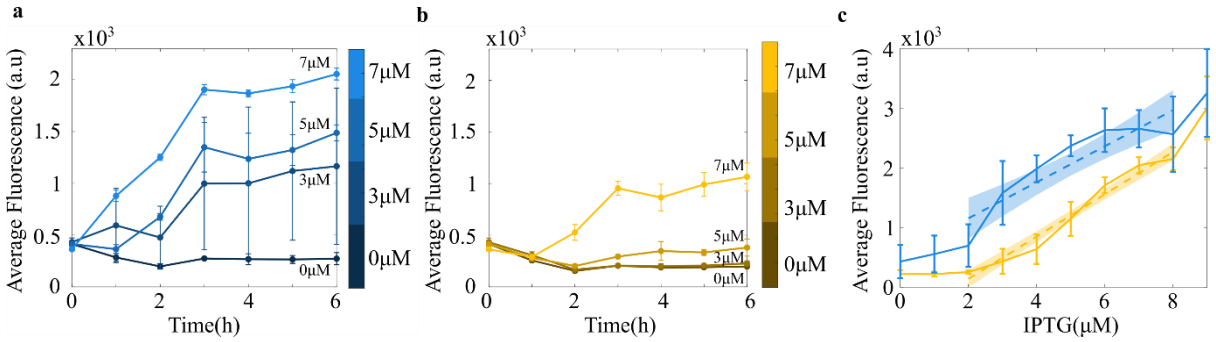


Figure 3 **Regulation of the targets fluorescence using open and closed loop control using controllers2.0/open loop controllers 2.0. a.** Average fluorescence of the targets over a 6h time course, using an open loop control architecture. The solid dots represent the average and the vertical bars the standard deviation of the data over n=3 biological replicates. Each trajectory is color coded and labelled with respect to the concentration of IPTG used in the experiment. **b.** Average fluorescence of the targets over a 6h time course, using a closed loop control architecture. The solid dots represent the average and the vertical bars the standard deviation of the data over n=3 biological replicates. Each trajectory is color coded and labelled with respect to the concentration of IPTG used in the experiment. **c.** Average steady state fluorescence of the targets over different IPTG concentrations. The blue (open loop) and yellow (closed loop) vertical bars are centered on the average values and their amplitude represented the standard deviation of the data over n=3 biological replicates. The dashed lines represent the linear interpolation of the data obtained with IPTG concentrations in the range $[2\ \mu M,\ 8\ \mu M]$. The shaded areas represent the confidence intervals of the linear model prediction. All steady states are collected after 6h from the initial inoculation.

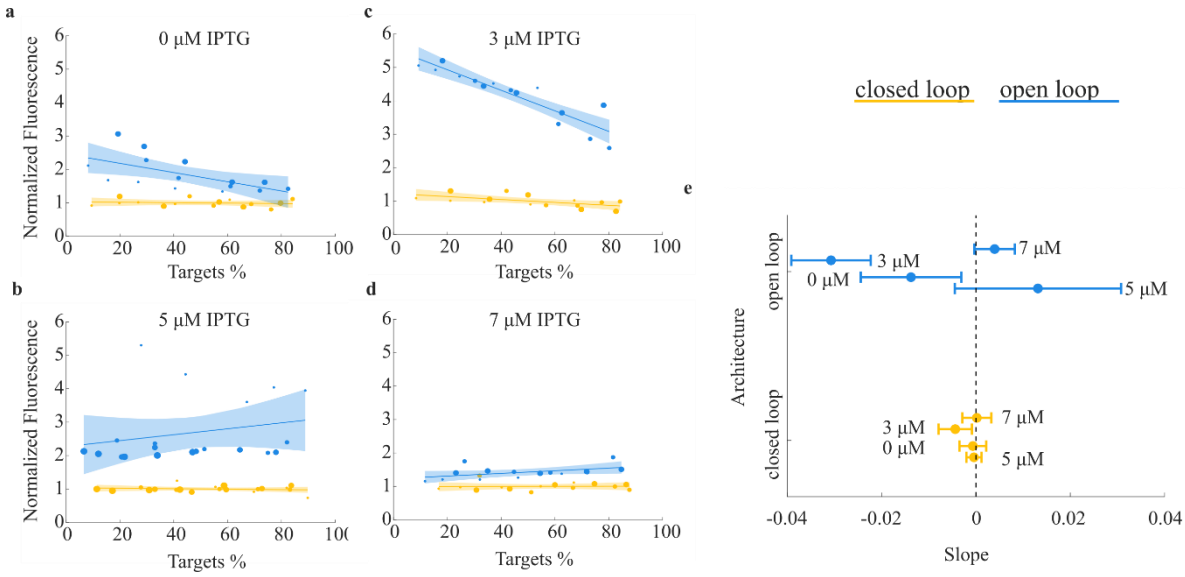


Figure 4 **Closed loop control robustness to changes consortium composition. a-d.** Normalized average fluorescence in open (blue) and closed (yellow) loop across different consortium compositions. The solid dots are the data collected over n=3 biological replicates. Dots of the same size belong to the same replica te. The data were fitted with a first order polynomial. The fitting and its confidence intervals are represented with the solid lines and the shaded areas, respectively. For each replicate, the data are normalized to the average fluorescence reached in closed loop across all compositions. **e.** Comparison of the estimates of the slopes of the linear fittings of data in panels **a-d** when a closed (yellow) or open (blue) loop architecture was used. The solid dots represent the slope estimates and the horizontal bars the 90% confidence interval on the estimates.